

Bright squeezed vacuum for two-photon spectroscopy: simultaneously high resolution in time and frequency, space and wavevector.

Paula Cutipa^{1,2,*} and Maria V. Chekhova^{1,2}

¹*Max-Planck Institute for the Science of Light, Staudtstraße 2, Erlangen D-91058, Germany*

²*University of Erlangen-Nuremberg, Staudtstraße 7/B2, 91058 Erlangen, Germany*

*Corresponding author: paula.cutipa@mpl.mpg.de

Entangled photons offer two advantages for two-photon absorption spectroscopy. One of them, the linear scaling of two-photon absorption rate with the input photon flux, is only valid at very low photon fluxes and is therefore impractical. The other is the overcoming of the classical constraints for simultaneous resolution in time-frequency and in space-wavevector. Here we consider bright squeezed vacuum (BSV) as an alternative to entangled photons. The efficiency increase it offers in comparison with coherent light is modest, but it does not depend on the photon flux. Moreover, and this is what we show in this work, BSV also provides simultaneously high resolution in time and frequency, and in space and wavevector. In our experiment, we measure the widths of the second-order correlation functions in space, time, frequency, and angle, and demonstrate the violation of the constraint given by the Fourier transformation, also known as the Mancini criterion of entanglement.

Entangled photons play an important role in different applications such as quantum imaging, microscopy, spectroscopy, and metrology [1, 2]. In particular, energy-time and position-momentum entanglement permits the enhancement of applications based on two-photon absorption (TPA), such as TPA spectroscopy for complex sample analysis or cellular imaging [3–8]. One of the advantages of using entangled photons is that it improves the TPA rate, which then scales with the photon flux linearly, and not quadratically, as in the case of coherent light [9, 10]. This happens because the TPA rate is proportional to the second-order correlation function (CF) of the incident light [11] at zero delay and displacement, $g^{(2)}(0)$, which for a weak flux of photon pairs scales inversely with the mean photon number [9].

This enables the analysis of biological samples at low light intensities, avoiding damage to the sample [3, 10]. However, this linear dependence is only valid at very low photon fluxes, where it can be hardly used in practice [6, 12].

Another advantage of using photon pairs for TPA spectroscopy is the simultaneously high and independent resolution in time ($\delta\tau$) and frequency ($\delta\omega$) they provide [4]. Indeed, photons entangled in time and frequency violate the classical relation $\delta\omega\delta\tau \geq 2\pi$, also known as the Mancini separability bound [13]. The same situation is valid for the transverse wavevector (δk) and space ($\delta\xi$) [14]. This enables simultaneously high resolution in time, space, frequency, and wavevector.

Entangled photons are usually generated by spon-

taneous parametric down-conversion (PDC). When strongly pumped, PDC produces a brighter state of light, bright squeezed vacuum (BSV) [15–18]. For this state, $g^{(2)}(0) = 3$, which provides only threefold enhancement of two-photon absorption compared to the case of coherent light excitation [19], but this enhancement is independent of the photon flux. Meanwhile, the mean number of photons per one mode of BSV, $N = \sinh^2(G)$, where G is called the parametric gain, can be as high as for laser sources. This makes BSV a prospective source for practical use in multiphoton absorption. Below we show that the second advantage of entangled photons, the simultaneously high resolution in time, space, frequency, and wavevector, is also valid for BSV.

The time, frequency, space, and wavevector resolution for two-photon transitions is determined by the second-order CF. The CF, in the general case, is a nonfactorable function of four variables: two time moments and two space positions (in one dimension, for simplicity), $g^{(2)}(t, t'; x, x')$ [17, 20, 21]. Alternatively, the CF can be considered as a function of frequencies and transverse wavevectors, $g^{(2)}(\omega, \omega'; k, k')$ [22].

At low parametric gain, $G \ll 1$, $g^{(2)}(0) \approx 1/G^2$ and is very high. The resolution provided by entangled photons in two-photon spectroscopy is given by its widths with respect to the corresponding variables: for instance, $\delta\tau$ is the width of $g^{(2)}(t, t'; x, x)$ at fixed t', x , and similarly with the other variables.

At high gain, $G \gtrsim 1$, photon pairs overlap, and their accidental coincidences, as well as thermal correlations of photons within one mode, start to play a role. Then, the value of $g^{(2)}$ reduces [9, 18], but its widths in time $\delta\tau$, space $\delta\xi$, frequency $\delta\omega$, and transverse wavevector δk , further called *correlation widths*, do not change much.

In this work we measure all these four widths. To measure $\delta\tau$ and $\delta\xi$, we build an ultra-fast autocorrelator based on sum-frequency generation (SFG) [17, 23] in a non-phase-matched crystal. By using type-II SFG we get rid of the first-order interference fringes [24]. The values of $\delta\omega$ and δk we obtain from the measurement of the covariance of BSV intensity [16, 25].

The experimental setup is displayed in Fig. 1. We

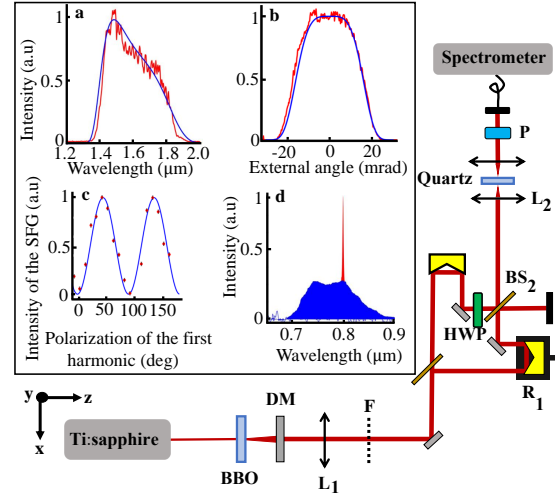


Figure 1: Experimental setup for measuring the second-order CF. We produced BSV in the BBO crystal whose output face was imaged on beam splitter BS_2 by lens L_1 and then on the quartz crystal by lens L_2 . In the autocorrelator, retroreflector R_1 scanned the time delay and beamsplitter BS_2 scanned the spatial displacement. In one arm, a HWP changed the polarisation, so that type-II SFG was generated in quartz at the output and registered, after polarizer P , by a spectrometer. The insets show the wavelength and angular spectra of BSV emitted via collinear degenerate PDC (a, b), the dependence of the SFG signal on the input polarization with one arm blocked (c) and the SFG spectrum (d).

generated BSV with an amplified Ti-sapphire laser (wavelength 800 nm, pulse duration 1.6 ps, repetition rate 5 kHz, mean power 1W, waist 0.8 mm) in a 10 mm β -barium-borate (BBO) crystal cut for type-I phase matching. The experiment was run at gain $G = 10$, both under collinear (the pump wavevector at 19.87° to the optic axis) and non-collinear (the pump wavevector at 19.93° to the optic axis) phase matching. In both cases, the angular-frequency spectrum of BSV is bounded, however, it is factorable only in the collinear configuration [26]. The optic axis of the BBO crystal was in the y-z plane (where walk-off occurred), the pump was polarized along the

y-direction, and the BSV along the x-direction. The pump radiation was rejected with dichroic mirrors DM and the BSV was collected with lens L_1 (focal length 15 cm), its Fourier plane shown by a dotted line (F). At this position we placed a spectrometer to measure the wavelength spectrum of the BSV. It was centered at 1600 nm, and under collinear phase matching it had a bandwidth of $\Delta\lambda = 360$ nm (Fig. 1 (a)). The angular spectrum, measured with a camera at the same position, is shown in Fig. 1 (b). In all further measurements, to get rid of the walk-off effect we reduced the angular spectrum in the y-z plane to 10 mrad by placing a 1.6 mm slit in plane F along the x-direction.

The BSV beam was then sent into the autocorrelator through a 50:50 beam splitter and the time delay was introduced in one arm by retroreflector R_1 . In the other arm, a broadband half-wave plate HWP changed the polarisation from ‘x’ to ‘y’. This modification eliminated the first-order interference at the output of the second beamsplitter BS_2 , where the two beams were combined. The spatial displacement was generated by moving BS_2 transversely to the beam propagation direction. Noteworthy, lens L_1 imaged the output face of the BBO crystal on BS_2 with an $M = 8$ magnification, which we took into account while measuring the width of the spatial correlation.

Further, lens L_2 imaged BS_2 on the SFG crystal, which was a 500 μm thick z-cut α -quartz. The SFG was non-phasedmatched [27], which made it broadband and let all frequency components of BSV contribute [17]. The dependence of the SFG signal on the input polarization (Fig. 1 (c)) is typical for type-II SFG, and it originates from the structure of the nonlinear tensor of quartz. As a result, there was no SFG from either arm of the autocorrelator, which had ‘x’ (0°) or ‘y’ (90°) polarization, but only from both. The SFG radiation was then collected and sent, after polarizer P, to a spectrometer. The SFG spectrum obtained for a perfectly balanced autocorrelator is shown in Fig 1 (d). The peak, known as the *coherent contribution*, is formed by merging photons from the same pair, and its area (red) corresponds to the real coincidences in a Hanbury Brown – Twiss (HBT) measurement. The background is caused by

photons from different pairs and its area (blue) corresponds to the ‘thermal’ and ‘accidental’ coincidences in a HBT setup [28, 29].

Frequency and wavevector correlations

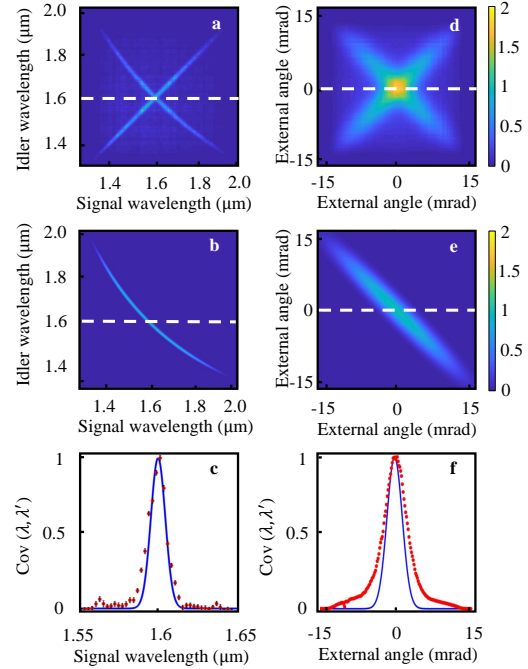


Figure 2: Intensity covariance measured versus wavelengths (a) and angles (d) and its cross-correlation part calculated for the same cases (b,e). Panels (c) and (f) show, respectively, cross-sections of panels (a,d) (points) and panels (b,e) (lines) at $\lambda = 1.6 \mu\text{m}$ and at $\theta = 0^\circ$ (white dashed lines), normalized to the maximum values

To find the frequency correlation width $\delta\omega$ of BSV, we obtained its spectra by placing a multimode fiber tip, connected to a spectrometer, in the Fourier plane (F in Fig 1). Instead of the CF $g^{(2)}(\omega, \omega')$ mentioned above, we measured the covariance [16, 30] of the

intensity $I(\lambda)$ at different wavelengths λ, λ' :

$$\text{Cov}(\lambda, \lambda') = \langle I(\lambda)I(\lambda') \rangle - \langle I(\lambda) \rangle \langle I(\lambda') \rangle. \quad (1)$$

This value is related to the CF $g^{(2)}(\lambda, \lambda')$ as $\text{Cov}(\lambda, \lambda') = \langle I(\lambda) \rangle \langle I(\lambda') \rangle (g^{(2)}(\lambda, \lambda') - 1)$. The frequency correlation width at wavelength λ is then $\delta\omega = 2\pi c\delta\lambda/\lambda^2$, where c is the speed of light and $\delta\lambda$ is the FWHM of the covariance distribution. Figure 2(a) shows the covariance calculated according to Eq. (1) from 4000 spectra obtained in the collinear configuration, each one acquired over 5 pulses. The shape seen along the main diagonal ($\lambda = \lambda'$) is caused by the auto-correlation of each frequency mode with itself. The shape along the anti-diagonal demonstrates the cross-correlations between signal and idler photons. The maxima follow the energy conservation condition, $\omega_p = \omega + \omega'$ (ω_p is the pump frequency), i.e., $\lambda^{-1} + \lambda'^{-1} = \text{const.}$ The normalization is chosen such that for both cross-correlation and anti-correlation part, the maximal value is unity. The FWHM of the covariance cross-section (panel (c), red points) yields the range of correlations $\delta\lambda = 12$ nm, corresponding to $\delta\omega = 8.8 \cdot 10^{12}$ Hz.

To calculate $\delta\omega$, we use the standard expression for the two-photon probability amplitude $F(\omega, \omega', k, k')$, where, to take into account the high-gain regime, the ‘sinc’ function is replaced by its hyperbolic analog [31, 32]:

$$F(\omega, \omega', k, k') = F_p(\omega + \omega' - \omega_p) F_p(k + k') \frac{G}{\tilde{G}} \sinh \tilde{G}. \quad (2)$$

Here, $F_p(\omega)$ and $F_p(k)$ are the pump Gaussian spectral and transverse wavevector amplitudes, respectively [33], $\tilde{G} \equiv \sqrt{G^2 - (\Delta(\omega, \omega', k, k'))^2 L^2/4}$, $\Delta(\omega, \omega', k, k')$ is the wavevector mismatch and L is the crystal length. In the high-gain regime of PDC, the pump pulse duration is effectively reduced (by a factor of 3.2 for $G = 10$) [25] because BSV is mainly generated around the pulse peak, and we take it into account by assuming that the pump spectrum broadens 3.2 times.

The cross-correlation part of the covariance was calculated as $|F(\omega, \omega', 0, 0)|^2$ and plotted in Fig. 2(b). Its cross-section (panel (c), blue line) gives the value of $\delta\lambda = 10$ nm. The somewhat larger value obtained

in experiment is due to the finite resolution of the spectrometer (7 nm).

A similar procedure was performed to find the angular width of correlations. We replaced the spectrometer with a camera preceded by a 12 nm band-pass filter centered at 1600 nm. From 9000 2D frames, each one acquired over 5 pulses, we selected the central rows to pass to 1D angular spectra and calculated the intensity covariance. The result is shown in Fig. 2 (d). As in the case of wavelengths, the angular distribution of the covariance shows the auto-correlation part (diagonal) and the cross-correlation part (anti-diagonal). Panel (e) of the same figure shows the calculated cross-correlation. Similarly to the case of wavelengths, the covariance was calculated as $|F(\omega_p/2, \omega_p/2, k, k')|^2$, with the effective narrowing of the pump beam waist by a factor of 3.2 taken into account. Panel (f) shows the cross-sections of the experimental (red points) and the calculation (blue line) distributions. The measured angular width of correlations is $\delta\theta = 4.1$ mrad, somewhat larger than the calculated value 3.4 mrad. The resulting width in the transverse wavevector is $\delta k = 0.016 \mu\text{m}^{-1}$.

Spatiotemporal correlations

We used the autocorrelator to measure the dependence of $g^{(2)}(t, t', x, x')$ on $\tau \equiv t - t'$ and $\xi \equiv x - x'$. For a fixed position of BS_2 we scanned the time delay in one arm with R_1 , similar to Ref. [34]. For each time delay τ between the two arms, we obtained a spectrum as shown in Fig. 1 (d). The height of the peak strongly depends on τ and becomes zero at large delays, indicating that only photons that belong to different pairs merge into a sum-frequency photon. From the spectra, we calculated the value of the CF, according to Ref. [35], as $g^{(2)}(\tau) = 2(B(\tau)/B_{max} + R(\tau)/B(\tau))$, where $R(\tau)$ is the integral spectrum of the peak (red area in Fig. 1 (d)), $B(\tau)$ the integral spectrum of the background (blue area in Fig. 1 (d)), and B_{max} its maximal value, which is achieved at $\tau = 0$.

This is how we obtained the 1-dimensional plot shown in Fig.3 (a) for $\xi = 0$. The correlation

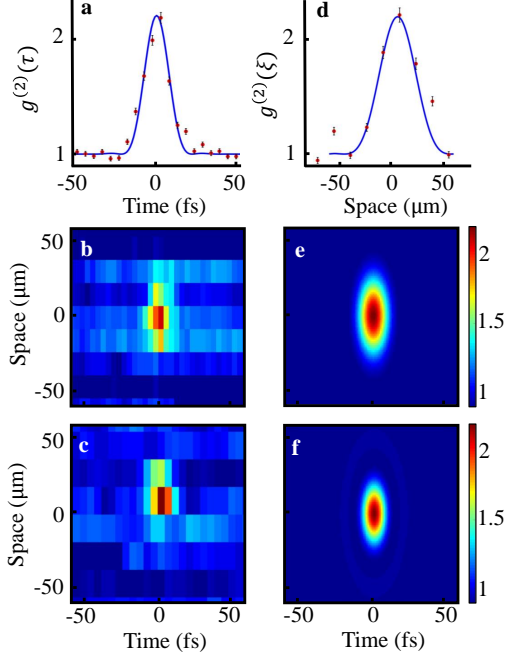


Figure 3: Second-order CF $g^{(2)}(\tau, \xi)$ measured (b,c) and calculated (e,f) for the collinear (b,e) and non-collinear (c,f) PDC. Panels (a) and (b) show the profiles of panels (b) (points) and (e) (line) at $\xi = 0$ and $\tau = 0$, respectively.

time $\delta\tau$ is equal to its full width at half maximum (FWHM). We repeated this measurement for each spatial displacement ξ made with BS_2 . Importantly, each spatial displacement generated an extra time delay, which we compensated by retroreflector R_1 . By stacking together $g^{(2)}(\tau)$ distributions at different ξ , we obtained the two-dimensional distribution $g^{(2)}(\tau, \xi)$ (Fig. 3) for both collinear (b) and non-collinear (c) PDC. Panels (e) and (f) show the corresponding theoretical distributions, calculated as squared two-dimensional Fourier transforms of Eq.(2). The distributions for the non-collinear configuration are narrower due to a broader wavelength-angular spectrum. In agreement with the theoretical calculation, the correlation time and distance for the collinear case are, respectively, 18 ± 2 fs and 45 ± 6 μm , and for the non-collinear case, 12 ± 2 fs and 33 ± 6

μm . The peak value $g^{(2)}(0, 0)$ obtained is 2.2 and not 3, as expected, due to the group-velocity dispersion in the optical elements. Panel (d) shows the space profile of the CF at $\tau = 0$ for collinear PDC: the points and the line are the cross-sections of panels (b) and (e), respectively.

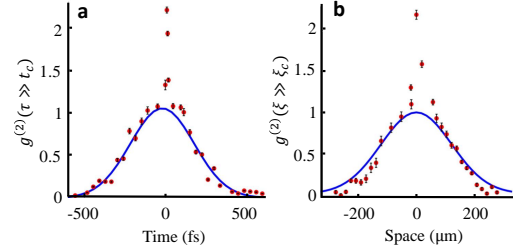


Figure 4: The CF $g^{(2)}(\tau)$ (a) and $g^{(2)}(\xi)$ (b) measured over larger time and space scales. The pedestals follow Gaussian distributions (blue lines) given by the BSV pulse duration (a) and beam waist (b).

Figure 3 shows the CF $g^{(2)}(\tau, \xi)$ distributions only in the vicinity of its maximum at $\tau = \xi = 0$. We also measured its behavior at a larger scale, with the results shown in Fig. 4 (a,b). The background follows a Gaussian distribution (blue line) whose widths in time and space are determined, respectively, by the BSV pulse duration and the beam waist. In agreement with the above-mentioned effect of the high gain, both widths are indeed 3.2 times smaller than those for the pump [18, 25, 36].

Finally, we calculate the time-frequency and space-wavevector products. For collinear degenerate PDC, we get $\delta\tau\delta\omega = 0.16$ and $\delta\xi\delta k = 0.72$. Both values are far below the Mancini (or Fourier) bound 2π . We note that the second condition, $\delta\xi\delta k \ll 2\pi$, was also demonstrated recently for BSV obtained through four-wave mixing, using noise reduction measurement [37].

In conclusion, we measured the the second-order CF for BSV as a function of space and time. We obtained the temporal and spatial correlation widths of $\delta\tau = 18$ fs and $\delta\xi = 45$ μm for the collinear degenerate configuration and $\delta\tau = 12$ fs and $\delta\xi = 33$ μm

for the non-collinear non-degenerate configuration, respectively. These values define the resolution for two-photon spectroscopy with BSV. The high temporal and spatial resolution is useful for analyzing complex samples and extracting information about their energy levels. In addition, we found the correlation widths of BSV in frequency and transverse wavevector, $\delta\omega = 8.8 \cdot 10^{12}$ Hz, $\delta k = 0.016 \mu\text{m}^{-1}$, respectively. As a result, we have demonstrated that BSV enables simultaneously high resolution in time and frequency, and space and wavevector.

We thank Tomás Santiago-Cruz for the help in experiment and Denis Kopylov for helpful discussions.

Funding.

P. Cutipa acknowledges the funding provided by the National Agency for Research and Development (ANID) / DOCTORADO BECAS CHILE/2017 - 72180453.

Disclosures.

The authors declare no conflicts of interest.

References

- [1] Alex S Clark et al. “Special Topic: Quantum sensing with correlated light sources”. In: *Applied Physics Letters* (2021).
- [2] Konstantin E Dorfman, Frank Schlawin, and Shaul Mukamel. “Nonlinear optical signals and spectroscopy with quantum light”. In: *Reviews of Modern Physics* 88.4 (2016), p. 045008.
- [3] Barak Dayan et al. “Nonlinear interactions with an ultrahigh flux of broadband entangled photons”. In: *Phys. Rev. Lett.* 94.4 (2005), p. 043602.
- [4] Frank Schlawin, Konstantin E Dorfman, and Shaul Mukamel. “Entangled two-photon absorption spectroscopy”. In: *Accounts of chemical research* 51.9 (2018), pp. 2207–2214.
- [5] Roberto de J León-Montiel et al. “Temperature-controlled entangled-photon absorption spectroscopy”. In: *Phys. Rev. Lett.* 123.2 (2019), p. 023601.
- [6] Alexander Mikhaylov et al. “A comprehensive experimental system for measuring molecular two-photon absorption using an ultrafast entangled photon pair excitation source”. In: *Advanced Optical Techniques for Quantum Information, Sensing, and Metrology* 11295 (2020), 112950Q.
- [7] Juan P Villabona-Monsalve, Ryan K Burdick, and Theodore Goodson III. “Measurements of Entangled Two-Photon Absorption in Organic Molecules with CW-Pumped Type-I Spontaneous Parametric Down-Conversion”. In: *The Journal of Physical Chemistry C* 124.44 (2020), pp. 24526–24532.
- [8] Dmitry Tabakaev et al. “Energy-time-entangled two-photon molecular absorption”. In: *Physical Review A* 103.3 (2021), p. 033701.
- [9] DN Klyshko. “Transverse photon bunching and two-photon processes in the field of parametrically scattered light”. In: *Sov. Phys. JETP* 56.4 (1982), p. 753.
- [10] Juha Javanainen and Phillip L Gould. “Linear intensity dependence of a two-photon transition rate”. In: *Physical Review A* 41.9 (1990), p. 5088.
- [11] Roy J Glauber. “The quantum theory of optical coherence”. In: *Physical Review* 130.6 (1963), p. 2529.
- [12] Michael G Raymer et al. “How large is the quantum enhancement of two-photon absorption by time-frequency entanglement of photon pairs?” In: *Optica* 8.5 (2021), pp. 757–758.
- [13] Stefano Mancini et al. “Entangling macroscopic oscillators exploiting radiation pressure”. In: *Physical Review Letters* 88.12 (2002), p. 120401.

- [14] John C Howell et al. “Realization of the Einstein-Podolsky-Rosen paradox using momentum-and position-entangled photons from spontaneous parametric down conversion”. In: *Physical Review Letters* 92.21 (2004), p. 210403.
- [15] Timur Iskhakov, Maria V Chekhova, and Gerd Leuchs. “Generation and direct detection of broadband mesoscopic polarization-squeezed vacuum”. In: *Physical Review Letters* 102.18 (2009), p. 183602.
- [16] K Yu Spasibko, T Sh Iskhakov, and Maria V Chekhova. “Spectral properties of high-gain parametric down-conversion”. In: *Optics Express* 20.7 (2012), pp. 7507–7515.
- [17] Enrico Brambilla et al. “Disclosing the spatiotemporal structure of parametric down-conversion entanglement through frequency up-conversion”. In: *Physical Review A* 85.6 (2012), p. 063834.
- [18] Alessia Allevi et al. “Coherence properties of high-gain twin beams”. In: *Physical Review A* 90.6 (2014), p. 063812.
- [19] Kirill Yu Spasibko et al. “Multiphoton effects enhanced due to ultrafast photon-number fluctuations”. In: *Physical Review Letters* 119.22 (2017), p. 223603.
- [20] L Caspani, E Brambilla, and A Gatti. “Tailoring the spatiotemporal structure of biphoton entanglement in type-I parametric down-conversion”. In: *Physical Review A* 81.3 (2010), p. 033808.
- [21] A Gatti et al. “X entanglement: the non-factorable spatiotemporal structure of biphoton correlation”. In: *Physical Review Letters* 102.22 (2009), p. 223601.
- [22] MA Finger et al. “Characterization and shaping of the time-frequency Schmidt mode spectrum of bright twin beams generated in gas-filled hollow-core photonic crystal fibers”. In: *Physical Review A* 95.5 (2017), p. 053814.
- [23] Barak Dayan et al. “Two photon absorption and coherent control with broadband down-converted light”. In: *Phys. Rev. Lett.* 93.2 (2004), p. 023005.
- [24] Fabien Boitier et al. “Two-photon-counting interferometry”. In: *Physical Review A* 87.1 (2013), p. 013844.
- [25] PR Sharapova et al. “Properties of bright squeezed vacuum at increasing brightness”. In: *Physical Review Research* 2.1 (2020), p. 013371.
- [26] Kirill Yu Spasibko et al. “Ring-shaped spectra of parametric downconversion and entangled photons that never meet”. In: *Opt. Lett.* 41.12 (2016), pp. 2827–2830.
- [27] Denis A Kopylov et al. “Study of broadband multimode light via non-phase-matched sum frequency generation”. In: *New Journal of Physics* 21.3 (2019), p. 033024.
- [28] Ottavia Jedrkiewicz et al. “High visibility pump reconstruction via ultra broadband sum frequency mixing of intense phase-conjugated twin beams”. In: *Optics Express* 19.14 (2011), pp. 12903–12912.
- [29] Izo Abram et al. “Direct observation of the second-order coherence of parametrically generated light”. In: *Physical Review Letters* 57.20 (1986), p. 2516.
- [30] Lina Beltran et al. “Orbital angular momentum modes of high-gain parametric down-conversion”. In: *Journal of Optics* 19.4 (2017), p. 044005.
- [31] Kirill Spasibko. “Spectral and statistical properties of high-gain parametric down-conversion”. In: *arXiv preprint arXiv:2007.12999* (2020).
- [32] Enrico Brambilla et al. “Simultaneous near-field and far-field spatial correlations in the high-gain regime of parametric down-conversion”. In: *Physical Review A* 69.2 (2004), p. 023802.

- [33] Yu M Mikhailova, PA Volkov, and MV Fedorov. “Biphoton wave packets in parametric down-conversion: Spectral and temporal structure and degree of entanglement”. In: *Physical Review A* 78.6 (2008), p. 062327.
- [34] Paula Cutipa, Kirill Yu Spasibko, and Maria V Chekhova. “Direct measurement of the coupled spatiotemporal coherence of parametric down-conversion under negative group-velocity dispersion”. In: *Optics Letters* 45.13 (2020), pp. 3581–3584.
- [35] Denis A Kopylov et al. “Spectral properties of second, third and fourth harmonics generation from broadband multimode bright squeezed vacuum”. In: *Laser Physics Letters* 17.7 (2020), p. 075401.
- [36] G. Brida et al. “Systematic study of the PDC speckle structure for quantum imaging applications”. In: *Journal of Modern Optics* 56.2-3 (2009), pp. 201–208. DOI: 10 . 1080 / 09500340802464665.
- [37] Ashok Kumar, Gaurav Nirala, and Alberto Marino. “Einstein-Podolsky-Rosen paradox with position-momentum entangled macroscopic twin beams”. In: *Quantum Science and Technology* (2021).